Analysis of Double-Output CLL Resonant Converter for All-Electric UAV Applications

Erdem Asa[1], Kerim Colak[2], Omer C. Onar[1], Dariusz Czarkowski[3], Burak Ozpineci[1]
[1]Oak Ridge National Laboratory, National Transportation Research Center, Tennessee, USA
[2]Hevo Power Inc., New York, USA
[3]New York University, Tandon School of Engineering, New York, USA

Abstract — **This paper presents a high-frequency isolated double-output resonant converter for unmanned aerial vehicle (UAV) applications. The proposed topology is established by using a full-bridge resonant inverter and double-output half-bridge active rectifiers. A phase-shifted pulse width modulation (PS-PWM) technique is utilized to adjusts the energy flow between output rectifiers in a wide voltage range regulation with a central control. The theoretical description of the converter is analyzed exploring the system model with a constant frequency under the different load conditions. The proposed system is validated with experimental results using 60 V input source and generating 0 - 100 V in each output at a full power of 500 W with 96% maximum efficiency in the laboratory experimental setup.**

Keywords— UAV, drone, battery, three-port, bi-directional, resonant, converter, power, energy, conversion.

I. Introduction

Unmanned aerial vehicles (UAVs) are broadly used by non-profit or profit defense and commercial platforms where they can take off or land vertically for surveillance and security, ground monitoring, last mile delivery, powerline inspection, and rescue operations after disasters, etc. [1]-[3]. The main challenge for these applications is the longer flight time at a low equipment cost [4]. Combustion engine-based propulsion system result in power fluctuations due to narrow peak efficiency range and suffer from low energy efficiency with high cost. Battery and energy storage and drive systems are crucial in avionic applications that all-electric propulsion can be achieved with higher efficient power conversion and control systems. Consequently, an all-electric propulsion system consists of a dc machine and battery energy storage system has been developed for future airplane platforms by NASA and Boeing recently [5]-[6]. An all-electric UAV system is illustrated in Fig. 1 with a battery pack and propulsion machines. Energy flow from the battery source to the loads is usually provided using non-isolated or isolated PWM dc-dc converters. For high operating frequency application, hard-switching causes high switching losses and typically requires an active clamp or snubber circuits across the switches. Due to their zero-current (ZCS) and/or zero-voltage switching (ZVS) characteristics through the entire load range, resonant converters are convenient topologies at high frequencies. Multi-output resonant converters might be useful to integrate the battery with the loads rather than using an individual converter in each stage. The advantages of multi-output converters are less passive components, high-power capability, high system efficiency, centralized control, and quick dynamic response.

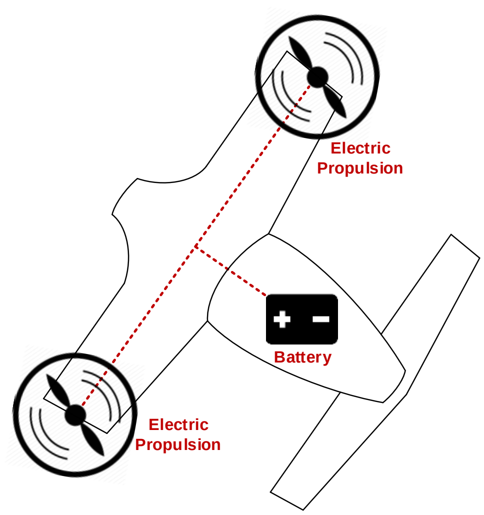

Fig. 1. All-electric UAV with two propulsion motors.

In the literature, several different multi-input-output resonant converter topologies have been presented [7]-[16]. An interleaved phase-shift modulation of three-port series resonant converter which is integrated to the grid with an additional inverter stage is demonstrated through a full-bridge rectifier at constant operating frequency in [7]. A new phase-shift PWM method is recommended for high-frequency multi-port applications in order to provide the synchronization between

This manuscript has been co-authored by Oak Ridge National Laboratory, operated by UT-Battelle, LLC, under Contract No. DE-AC05-00OR22725 with the U.S. Department of Energy. The United States Government retains and the publisher, by accepting the article for publication, acknowledges that the United States Government retains a non-exclusive, paid-up, irrevocable, world-wide license to publish or reproduce the published form of this manuscript, or allow others to do so, for United States Government purposes. The Department of Energy will provide public access to these results of federally sponsored research in accordance with the DOE Public Access Plan (http://energy.gov/downloads/doe-public-access-plan).

parallel resonant inverters in [8]. The magnitude and phase control of the system in steady state are also accomplished independently. Using a single three-winding transformer with active full-bridge, an isolated high-frequency three-port series resonant converter is introduced in [9]. Centralized control of bi-directional energy conversion can be achieved between proposed system active converter ports. The power management of energy sources in real time is investigated using a bidirectional isolated three-port resonant converter in [10]. The proposed parallel compensation of resonant converter system can manage the multiple loads and sources with different amplitude of voltage and current levels. Multiple port CLL resonant converter is introduced with a phase-shift in [11]-[13], an asymmetrical PWM technique in [14]-[15], and hybrid regulation with together of phase-shift and asymmetrical PWM in [16]-[17].

In this study, a double-output high-frequency isolated resonant converter is investigated for UAV applications. PS-PWM control is used to provide power flow regulation between the output ports. The proposed topology is operated at constant frequency and variable output voltage can be ensured in each output port for varying load characteristics. The CLL resonant converter might be a good alternative to the other isolated converters considering an air-gapped transformer using toroidal core that provides less magnetic losses and high-efficiency without any air gap. Toroidal core transformer with a parallel inductor is used to simplify the design process and reduce the magnetic losses in this work. Due to the large magnetizing inductance, the proposed system also provides to drive load active switches easier such that the current in each port is almost in phase. Without using any additional converter stages, the power flow control can be achieved between output active rectifiers from battery source. The central controller can be used instead of using individual controllers for each port without the need for communication devices or interfaces between controllers. The proposed system's analytical model is derived, and the system performance is validated with experimental results by testing a 500 W prototype with a maximum efficiency of 96% in the laboratory conditions. Related circuit analysis and the theoretical analysis with experimental validation of the converter are discussed in details in following section.

II. Circuit Model and Theoretical Analysis of The Proposed Converter

The proposed system topology with double-output converter is shown in Fig. 2. It consists of a primary full-bridge dc-ac resonant inverter, a series connected two transformers in the primary, and two-stage output with two separate half-bridge resonant active rectifiers on the secondary sides. The resonant tank components include capacitors C_{S1} and C_{S2}, parallel inductances L_{S1} and L_{S2}, and isolated transformers T_1 and T_2 as seen from Fig. 2. The phase-shift angle controls the output power flow between output rectifiers by switching secondary side active-rectifiers with respect to the primary side full-bridge resonant inverter.

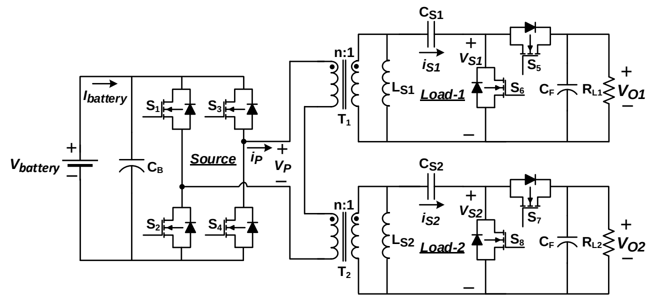

Fig. 2. Proposed isolated three-port resonant converter.

The equivalent circuit and simplified models of the proposed system can be presented from the primary side in Fig. 3 (a) and Fig. 3 (b) by using the fundamental harmonic approximation (FHA). The equivalent circuit parameters in Fig. 3 (a) consist of the input voltage source V_P, the equivalent load impedances Z_{i1} and Z_{i2}, resonant capacitors C_{P1} and C_{P2}, parallel inductances L_{P1} and L_{P2}, and transformer model L_{T1}, L_{T2}, where $L_{T1}=\{L_{LKP1}+L_{LKS1}^*\}$, $L_{T2}=\{L_{LKP2}+L_{LKS2}^*\}$ as shown in Fig. 3 (b).

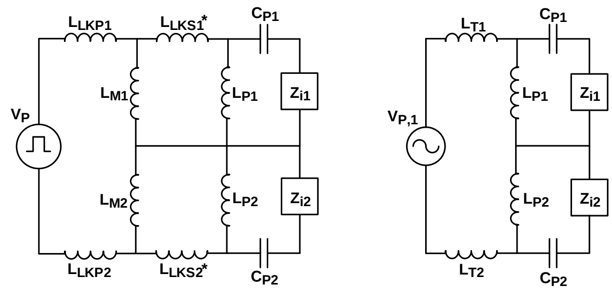

(a) (b)

Fig. 3. The proposed converter: equivalent circuit (a) and simplified model (b).

The primary-side full-bridge resonant inverter can be described using FHA analysis,

$$v_P(t) = \begin{cases} V_{battery}, 0 < \omega t \le \pi \\ -V_{battery}, \quad \pi < \omega t \le 2\pi \end{cases} \tag{1}$$

where the phase-shift function between the full-bridge resonant inverter legs is constant and considered to be *180* degrees. The fundamental components of the voltages $v_{P,1(t)}$ can be specified in the phasor domain as

$$V_{P,1} = \frac{4}{\pi} V_{battery} \tag{2}$$

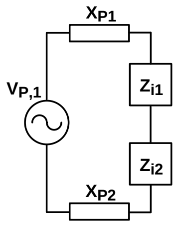

Fig. 4. Single -phase equivalent model of the proposed converter.

The equivalent model can be simplified to a single-phase circuit as shown in Fig. 4, where the resonant equivalent impedances X_{P1}, and X_{P2}, and the input equivalent impedances Z_{i1} and Z_{i2} can be described as,

$$X_{P1} = j\omega L_{T1} + \left[j\omega L_{P1} // \left(\frac{1}{j\omega C_{P1}} + Z_{i1} \right) \right] \tag{3}$$

$$X_{P2} = j\omega L_{T2} + \left[j\omega L_{P2} // \left(\frac{1}{j\omega C_{P2}} + Z_{i2} \right) \right] \tag{4}$$

$$Z_{i1} = \frac{2n^2 R_{L1}(cos\theta_1[cos\theta_1 + jsin\theta_1])}{\pi^2} \tag{5}$$

$$Z_{i2} = \frac{2n^2 R_{L2}(cos\theta_2[cos\theta_2 + jsin\theta_2])}{\pi^2} \tag{6}$$

where θ_1 and θ_2 are the phase angle of the half wave rectifiers in the secondary side between voltage and current, and n and R_{L1} are transformer turns ratio and load resistance of the converter, respectively.

In order to describe the power flow, the following general equations can be written by using the primary and secondary-side current flow parameters as shown in Fig. 3 (b):

$$\begin{aligned} v_{P1} = i_P\left(\textstyle\sum_{k=1}^{2} j\omega L_{Tk} + \sum_{k=1}^{2} j\omega L_{Pk}\right) + \\ -i_{i1} j\omega L_{P1} - i_{i2} j\omega L_{P2} \end{aligned} \tag{7}$$

$$0 = -i_P j\omega L_{P1} + i_{i1}\left(j\omega L_{P1} + \frac{1}{j\omega C_{P1}} + Z_{i1} \right) \tag{8}$$

$$0 = -i_P j\omega L_{P1} + i_{i1}\left(j\omega L_{P1} + \frac{1}{j\omega C_{P1}} + Z_{i1} \right) \tag{9}$$

The described function can be rewritten in a matrix form by

$$\begin{bmatrix} V_{i,1} \\ 0 \\ 0 \end{bmatrix} = \begin{bmatrix} j\omega(L_{T1} + L_{T2} + L_{P1} + L_{P2}) & -j\omega L_{P1} & -j\omega L_{P2} \\ -j\omega L_{P1} & j\omega L_{P1} + \frac{1}{j\omega C_{P1}} + Z_{i1} & 0 \\ -j\omega L_{P2} & 0 & j\omega L_{P2} + \frac{1}{j\omega C_{P2}} + Z_{i2} \end{bmatrix} \begin{bmatrix} I_P \\ I_{i1} \\ I_{i2} \end{bmatrix} \tag{10}$$

The primary resonant current I_P and the secondary side currents I_{i1}, I_{i2} can be expressed by

$$I_P = \frac{V_{i,1} Z_1 Z_2}{Y} \tag{11}$$

$$I_{i1} = \frac{V_{i,1}(j\omega L_{P1}) Z_2}{Y} \tag{12}$$

$$I_{i2} = \frac{V_{i,1}(j\omega L_{P2}) Z_1}{Y} \tag{13}$$

where Z_1, Z_2, and Y can be described as

$$Z_1 = j\omega L_{P1} + \frac{1}{j\omega C_{P1}} + Z_{i1} \tag{14}$$

$$Z_2 = j\omega L_{P2} + \frac{1}{j\omega C_{P2}} + Z_{i2} \tag{15}$$

$$\begin{aligned} Y = Z_1(j\omega L_{P2})^2 + Z_2(j\omega L_{P1})^2 + \\ -j\omega(L_{P1} + L_{P2} + L_{T1} + L_{T2}) Z_1 Z_2 \end{aligned} \tag{16}$$

The equivalent resistances value can be obtained by taking the real component of (5) and (6), as

$$R_{i1} = \frac{2n^2 R_{L1}(cos^2\theta_1)}{\pi^2} \tag{17}$$

$$R_{i2} = \frac{2n^2 R_{L2}(cos^2\theta_2)}{\pi^2} \tag{18}$$

Taking imaginary portion of the equivalent impedances, the corresponding reactance values are defined as

$$X_{L1} = \frac{n^2 R_{L1}(jsin2\theta_1)}{\pi^2} \tag{19}$$

$$X_{L2} = \frac{n^2 R_{L2}(jsin2\theta_2)}{\pi^2} \tag{20}$$

Consequently, the output voltages $V_{O,1}$, $V_{O,2}$ and output powers $P_{O,L1}$, $P_{O,L2}$ delivered to the loads can be found as

$$V_{O,1} = \frac{|I_{i1}| cos^2\theta_1}{\pi^2} R_{L1} \tag{21}$$

$$P_{O,L1} = V_{O,1} I_{S1} \tag{22}$$

$$V_{O,2} = \frac{|I_{i2}| cos^2\theta_2}{\pi^2} R_{L2} \tag{23}$$

$$P_{O,L2} = V_{O,2} I_{S2} \tag{24}$$

The total input power $P_{i,T}$ can be obtained by

$$P_{i,T} = P_{O,L1} + P_{O,L2} = I_{S1}^2 R_{L1} + I_{S2}^2 R_{L2} \tag{25}$$

The power flow is illustrated for the input source as a function of the phase-shift angles in Fig. 5 (a), and the output powers are shown in Fig. 5 (b) and (c). As seen from Fig. (5), the output powers can be regulated from main source to the load at a desired value by controlling the phase shift angles of θ_1 and θ_2.

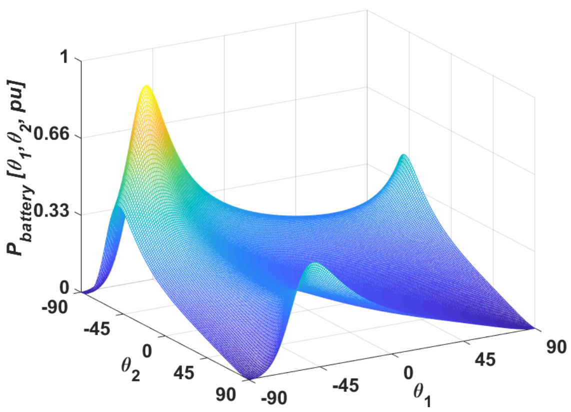

(a)

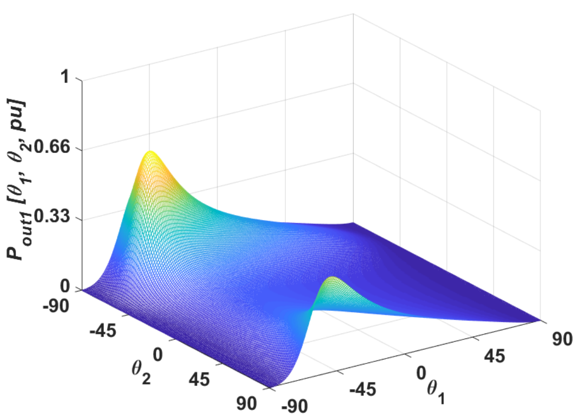

(b)

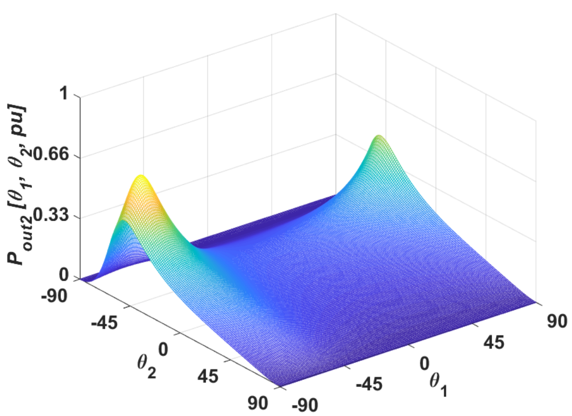

(c)

Fig. 5. The power flow for input power source (a), the first port output power (b), and the second outut power (c), with respect to the phase angles θ_1 and θ_2.

III. Experimental Results

The proposed technology is experimented for 500 W power, 60 V input voltage, and 0 - 100 V / 0 - 100 V controllable output voltage values with a laboratory get setup. The proposed system parameters are given in Table I. The converter input and output voltage / current waveforms are measured with a Rigol DS1054Z oscilloscope. The input and output power values are measured by a Yokogawa PZ4000 power analyzer.

TABLE I - The Proposed Converter Parameters

Symbol	Parameter	Values
$V_{battery}$	dc input voltage	60 V
V_{O1}, V_{O2}	dc output voltage range	0 – 100 V
I_{O1}, I_{O2}	output current range	0 – 2.5 A
P_{O1}, P_{O2}	rated power	500 W
C_{S1}, C_{S2}	resonant capacitor	60 nF
L_{S1}, L_{S2}	parallel inductance	24 uH
L_{lk}	transformer leakage inductance	30 uH
L_M	transformer mag. inductance	780 uH
f	operating frequency	190 kHz
Tr	transformer core	Toroid OP48020EC
n	transformer turns ratio	1:1
S	main switch	IRFP4227PbF
t_{dead}	dead time	300 ns

In order to prove the concept and demonstrate the operating principle, double-output synchronous half-wave rectifier is implemented as shown in Fig. 6. Phase-shift function determines the output power at each output load terminal based on the reference output values as shown in this scheme. The power flow can also be managed regulating the phase shift between output ports. The control modulation is implemented using field programmable gate array (FPGA) Spartan 6 XC6SLX9 and microprocessor STM32F407VG. The FPGA mainly ensures PWM phase-shift function with sensing the phase in each output port. Then, the phase-shift modulation is carried out to the MCU.

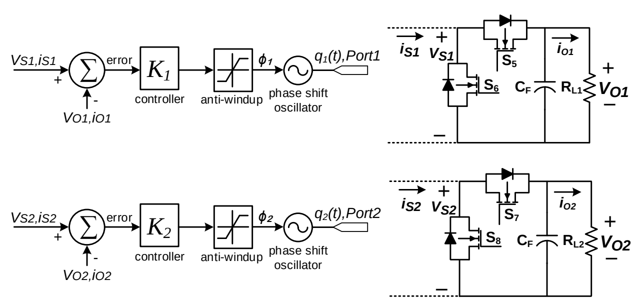

Fig. 6. Output power control for the output ports of the poposed system with phase-shift control modulation.

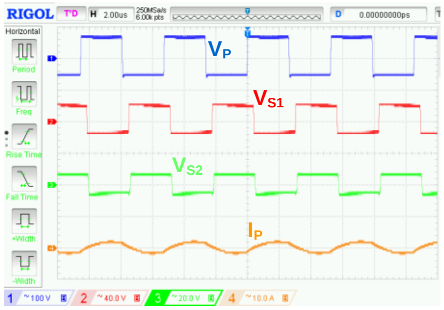

a) $\phi 1$=30º and $\phi 2$=30º for 10/30 Ω

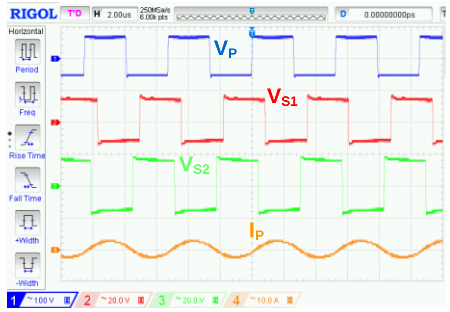

b) $\phi 1$=60º and $\phi 2$=30º for 20/20 Ω

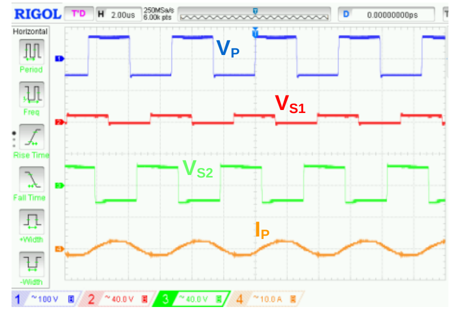

c) $\phi 1$=90º and $\phi 2$=30º for 30/10 Ω

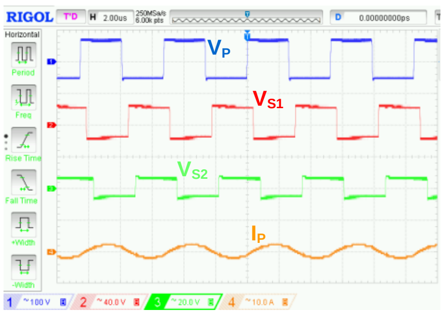

d) $\phi 1$=30º and $\phi 2$=60º for 10/30 Ω

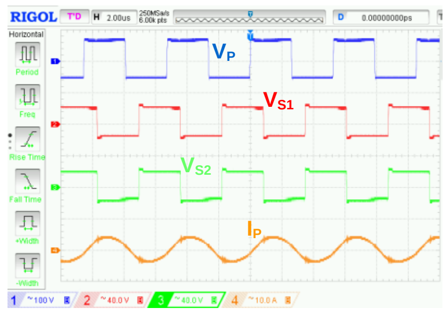

e) $\phi 1$=60º and $\phi 2$=60º for 20/20 Ω

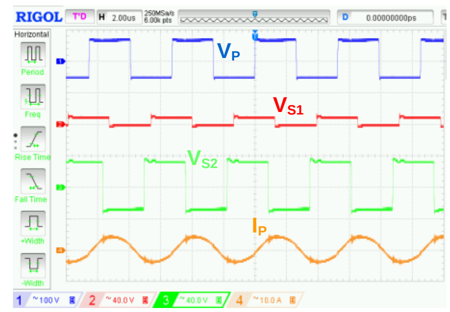

f) $\phi 1$=90º and $\phi 2$=60º for 30/10 Ω

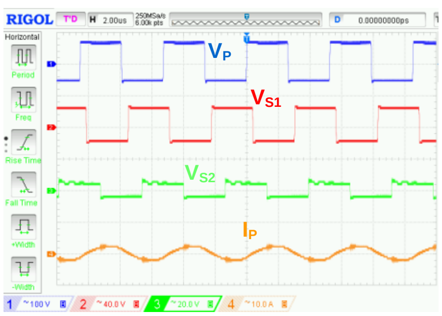

g) $\phi 1$=30º and $\phi 2$=90º for 10/30 Ω

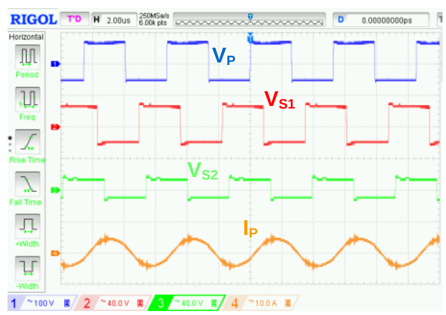

h) $\phi 1$=60º and $\phi 2$=90º for 20/20 Ω

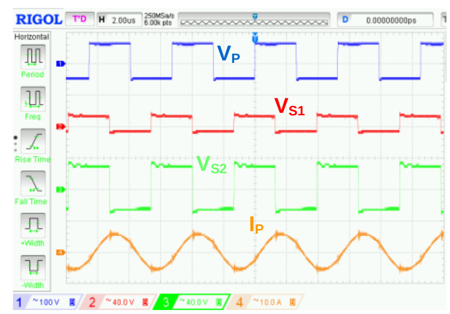

i) $\phi 1$=90º and $\phi 2$=90º for 30/10 Ω

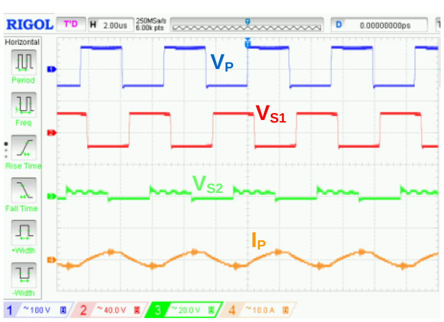

j) $\phi 1$=30º and $\phi 2$=120º for 10/30 Ω

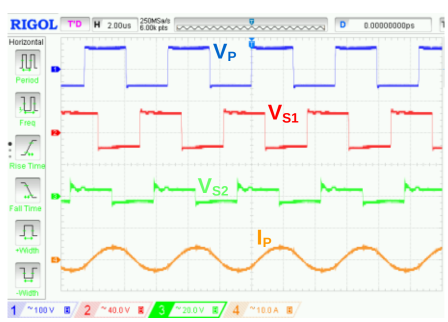

k) $\phi 1$=60º and $\phi 2$=120º for 20/20 Ω

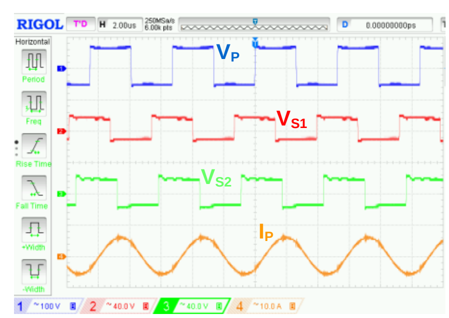

l) $\phi 1$=90º and $\phi 2$=120º for 30/10 Ω

Fig. 7. Primary and secondary side resonant tank voltages V_P, V_{S1}, V_{S2} and primary current I_P waveforms.

Primary and secondary voltage and current measurements are presented for the given for phase shift values ϕ_1 *(=30º, 60º, 90º,and 120º)* and $\phi 2$ *(=30º, 60º, 90º, and 120º)*, and different load conditions *(=10 / 30 Ω, 20 / 20 Ω, and 30 / 10 Ω)* in Fig. 7. Under different load conditions, it is shown that the phase angles θ_1 and θ_2 can be varied by the active switches in order to regulate the power flow control. By this way, power transfer with different combinations can be achieved between input and outputs.

V. CONCLUSIONS

In this study, a new double-output isolated resonant converter is presented for UAV applications. With the proposed secondary side active switches, a wide voltage regulation can be achieved between outputs by using the phase shift control angle. Novel converter topology has reduced number of active stages compared to the existing solutions. The converter model's theoretical analysis is presented using FHA and simplified circuit analysis. The system transfer function is derived by providing the equivalent circuit of the topology. By using a single dc voltage source at the input, experimental results are obtained with the maximum 96% efficiency. The source voltage is 60 V and output voltages and currents ranges are 0 to 100 V / 0 to 2.5 A, respectively. The experimental results prove that the proposed system provides a wide voltage regulation with the phase shift angle control of each of the outputs.

REFERENCES

[1] M. Aghaei, F. Grimaccia, C. A. Gonano, S. Leva, "Innovative automated control system for PV fields inspection and remote control," *IEEE Trans. Ind. Electron.*, vol. 62, no. 11, pp. 7287-7296, Nov. 2015.

[2] J. J. Cooley, P. Lindahl, C. L. Zimmerman, M. Cornachione, G. Jordan, S. R. Shaw, S. B. Leeb, "Multiconverter system design for fuel cell buffering and diagnostics under UAV load profiles," *IEEE Trans. Power Electron.*, vol. 29, no. 6, pp. 3232-3244, Jun. 2014.

[3] J. M. Arteaga, S. Aldhaher, G. Kkelis, C. Kwan, D. C. Yates, P. D. Mitcheson, "Dynamic capabilities of multi-MHz inductive power transfer systems demonstrated with batteryless drones," *IEEE Trans. Power Electron.*, vol. 34, no. 6, pp. 5093-5104, Jun. 2019.

[4] E. Bertran, A. Sànchez Cerdà, "On the trade-off between electrical power consumption and flight performance in fixed-wing UAV autopilots," *IEEE Trans. Veh. Technol.*, vol. 65, no. 11, pp. 8832-8840, Nov. 2016.

[5] D. L. Hall, J. C. Chin, A. D. Anderson, J. T. Thompson, A. D. Smith, R. D. Edwards, K. P. Duffy, "Development of a Maxwell X-57 High Lift Motor Reference Design," *AIAA/IEEE Electric Aircraft Technologies Symposium (EATS)*, pp. 1-24, 2019, Indianapolis, IN

[6] M. Duffy, A. Sevier, R. Hupp, E. Perdomo, S. Wakayama, "Propulsion Scaling Methods in the Era of Electric Flight," *AIAA/IEEE Electric Aircraft Technologies Symposium (EATS)*, pp. 1-23, 2018, Cincinnati, OH.

[7] I. J. Pitel, "Phase-modulated resonant power conversion techniques for high-frequency link inverters," *IEEE Trans. Ind. Appl.*, vol. IA-22, no. 6, pp. 1044-1051, Nov. 1986.

[8] J. Liu, K. W. E. Cheng, J. Zeng, "A unified phase-shift modulation for optimized synchronization of parallel resonant inverters in high frequency power system," *IEEE Trans. Ind. Electron.*, vol.61, no.7, pp. 3232-3247, Jul. 2014.

[9] H. Krishnaswami, N. Mohan, "Three-port series-resonant DC–DC converter to interface renewable energy sources with bidirectional load and energy storage ports," *IEEE Trans. Power Electron.*, vol. 24, no. 10, pp. 2289-2297, Oct. 2009.

[10] J. Zeng, W. Qiao, L. Qu, "An isolated three-port bidirectional dc-dc converter for photovoltaic systems with energy storage*," IEEE Trans. Ind. Appl.*, vol.51, no.4, pp.3493-3503, Jul./Aug. 2015.

[11] E. Asa, K. Colak, D. Czarkowski, "Analysis of a novel interleaved CLL resonant converter for EV battery charger applications," *IEEE Energy Conversion Congress and Exposition*, pp. 2031-2036, 2014, Pittsburgh, PA,

[12] E. Asa, K. Colak, D. Czarkowski, B. Ozpineci, "Analysis of High Frequency AC Link Isolated Three Port Resonant Converter for UAV Applications," *IEEE Applied Power Electronics Conference and Exposition*, pp. 1-6, 2020, New Orleans, LA

[13] E. Asa, K. Colak, D. Czarkowski, B. Ozpineci, "Analysis of High Frequency AC Link Isolated Three Port Resonant Converter for UAV Applications," IEEE Applied Power Electronics Conference and Exposition (APEC), New Orleans, LA, USA, 2020, pp. 1679-1684.

[14] D. J. Tschirhart, P. K. Jain, "A CLL resonant asymmetrical pulsewidth-modulated converter with improved efficiency," *IEEE Trans. Ind. Electron.*, vol.55, no.1, pp.114-122, Jan. 2008.

[15] K. Colak, E. Asa, M. Bojarski, D. Czarkowski, "Asymmetrical duty-cycle control of a novel multi-port CLL resonant converter," *IEEE Applied Power Electronics Conference and Exposition*, Charlotte, NC, 2015, pp. 3019-3024.

[16] S. H. Ryu, D. H. Kim, M. J. Kim, J. S. Kim, B. K. Lee, "Adjustable frequency-duty-cycle hybrid control strategy for full-bridge series resonant converters in electric vehicle chargers," *IEEE Trans. Ind. Electron.*, vol.61, no.10, pp.5354-5362, Oct. 2014.

[17] E. Asa, K. Colak, M. Bojarski, D. Czarkowski, "Asymmetrical Duty-Cycle and Phase-Shift Control of a Novel Multiport CLL Resonant Converter," *IEEE Journal of Emerging and Selected Topics in Power Electronics*, vol. 3, no. 4, pp. 1122-1131, Dec. 2015.